Effect of oxygen transfer on yeast growth – growth kinetic and reactor model to estimate scale-up effects in bioreactors

Petri Tervasmäki*[1], Marko Latva-Kokko[2], Sanna Taskila[1], Juha Tanskanen[1]

[1]University of Oulu, Chemical Process Engineering, P.O. Box 4300, FI-90014 Oulun yliopisto, Finland
[2]Outotec Oyj, Outotec Research Center, P.O. Box 69, FI-23101 Pori, Finland
*Corresponding author, petri.tervasmaki@oulu.fi, +358 40 5474973

Abstract

Large scale fermentations face challenges in mixing and mass transfer as well as in the design and construction of the equipment. Scale-up from laboratory and pilot scale experiments is difficult because different phenomena – such as mixing times and mass transfer conditions – scale in a different way.

We study the effect of mass transfer, reactor type and scale on the growth of *Pichia pastoris* yeast. Batch cultivation experiments monitoring the cell growth and ethanol formation are conducted in laboratory scale in two reactor types – stirred tank and an Outotec OKTOP®9000 draft tube reactor. Model for the yeast growth – including respirative and fermentative metabolism and the effect of dissolved oxygen – is formed based on literature. For scale-up studies, the growth model is used along with one dimensional reactor model that accounts for liquid mixing, gas phase dynamics and local gas hold-up and mass transfer coefficient.

By using a realistic growth model along with the reactor model, the simulated effects of scale-up are presented in terms of cell yield. A decrease in yield is noticed due to oxygen depletion in gas and insufficient liquid mixing. Potential improvements are related to the gas handling capacity and liquid mixing of the reactor.

Keywords

Scale-up; Mass transfer; Bioreactor; Stirred tank; Draft tube; Model

Nomenclature

a	Volumetric mass transfer area ($m^2\ m^{-3}$)
c_i	Concentration of component i ($g_i\ l^{-1}$)
D	Dilution rate (h^{-1})
D_L	Diffusion coefficient ($m^2\ s^{-1}$)
d_b	Bubble size (m)
EF_g	Exchange flow in gassed conditions ($m^3\ s^{-1}$)
F	Flow rate ($l\ h^{-1}$ or $m^3\ s^{-1}$)
H	Height of liquid in reactor (m)
IF	Induced flow ($m^3\ s^{-1}$)
k_H	Henry's constant for oxygen
k_L	Liquid side mass transfer coefficient ($m\ s^{-1}$ or $m\ h^{-1}$)
K_e	Saturation coefficient for ethanol uptake ($g_e\ l^{-1}$)
K_g	Saturation coefficient for glucose uptake ($g_g\ l^{-1}$)
K_i	Inhibition constant for glucose inhibition of ethanol uptake ($g_g\ l^{-1}$)
K_o	Saturation coefficient for oxygen uptake ($g_o\ l^{-1}$)
N_P	Impeller power number (-)
P	Pressure (Pa) or power (W)
p	Partial pressure (Pa)
q_i	Specific rate of component i ($g_i\ g_x^{-1}\ h^{-1}$)
V	Volume (l or m^3)
v_s	Superficial gas velocity ($m\ s^{-1}$)
y	Mole fraction (-)
Y_{ij}	Yield coefficient for components i and j ($g_i\ g_j^{-1}$)
z	Axial coordinate of reactor (z = 0 at the bottom) (m)

Greek letters

η	Viscosity (Pa s)
μ	Growth rate (h^{-1})
ρ	Density ($kg\ m^{-3}$)
τ	Gas phase residence time (s or h)
ϕ	Gas volume fraction (-)

Subscripts and superscripts

e	ethanol
ferm	fermentative pathway
g	glucose
gas	gas phase
o	oxygen
ox	oxidative pathway
sat	saturation concentration
x	cells

1 Introduction

The majority of industrial microbial processes are aerobic, meaning that the cells consume oxygen for cellular respiration. Due to the low solubility of oxygen in aqueous solutions, oxygen needs to be continuously dissolved from gas to the liquid phase by introducing air or another gas containing oxygen into the reactor. Ideally, the oxygen transfer rate of the reactor is sufficient to maintain the dissolved oxygen concentration above a critical value, thus matching the oxygen uptake rate of the cells. There are complex interactions between the hydrodynamics of the reactor, mass transfer parameters, and microbial growth. (Garcia-Ochoa et al., 2010; Garcia-Ochoa and Gomez, 2009)

Simple scale-up rules and related correlations are frequently discussed in the literature. One popular approach is correlations based on the mixing power per liquid volume to maintain similar values for overall volumetric mass transfer coefficient, $k_L a$. As pointed out by Nauha et al., (2015); the exponents in the common correlations are scale-dependent which limits their applicability in scaling up industrial processes. They also pointed out issues related to hydrodynamic regimes and oxygen mass balance in industrial scale aerobic fermentations.

Gas sparged below the impeller of a stirred tank reactor forms cavities behind the low pressure areas of the impeller blades. Depending on the impeller geometry and rotation rate as well as the gas flow rate, gas is dispersed by the impeller with varying efficiency. Flow regimes at the impeller can be roughly categorized, with increasing dispersion efficiency, to flooding, loading and complete recirculation. (Paul et al., 2004) However, even with sufficient gas dispersion by the impeller, high gas flow rates may cause a transition from homogeneous to heterogeneous flow regime, which is characterized by formation of large bubbles and bimodal bubble distribution. The flow in heterogeneous regime is more controlled by the gas flow rate. The transition depends mainly on the superficial gas velocity and occurs approximately at v_s = 0.03 m/s. (Gezork et al., 2000)

The superficial gas velocity is also present in many correlations, and it is often used to estimate the gas flow rate in different scales. If the gas flow is scaled by constant v_s, volumetric gas flow related to liquid volume, expressed as volume gas per volume liquid per minute (VVM), decreases as it scales by $V^{-1/3}$. When considering the stoichiometry in the process, maintaining constant VVM would be

advantageous. However, the maximum value for v_s to maintain a homogeneous flow regime that is controlled by the agitator is considered to be about 0.03 m s^{-1}. Therefore, due to a decreased VVM-value in large reactors, gas phase residence time increases with scale, and gas phase depletion is more significant. This decreases the driving force for mass transfer, which may lead to mass transfer limited conditions.

The effect of hydrostatic pressure on the flow regime is also notable in large vessels with high aspect ratios. At higher pressure, the conditions controlling homogeneous/heterogeneous transition conditions are different, due to increased gas density. Therefore, it may be that flow in the bottom part is homogeneous and transition to heterogeneous flow regime occurs in the higher parts of the reactor. The effect may be similar for the flooding/loading transition of the impellers. (Nauha et al., 2015) The flooding regime of the impellers, however, needs to be distinguished from the homogeneous/heterogeneous flow regime, and it is affected by gas flow rate and the diameter, revolution rate and geometry of the impeller.

The applicability of stirred draft tube reactors (SDTR) on microbial fermentations has been shown in previous studies (Moo-Young et al., 1993; Pollard et al., 1997). In addition, different SDTR designs have been compared to airlift (ALR, Chisti and Jauregui-Haza, 2002) and stirred tank reactors (STR, Lueske et al., 2015) in mixing and mass transfer studies. The SDTR was found to have higher efficiency for mass transfer compared to STR but not to ALR. Recently, a scaled down model of industrial scale bottom-agitated draft tube reactor (Outotec OKTOP®9000) was shown to perform well in mixing and mass transfer experiments and was also suitable for cell cultivations (Tervasmäki et al., 2016). This reactor type has been used in the hydrometallurgical industry for direct leaching of zinc concentrate in scales up to 1000 m^3, which is a rather large scale for multiphase stirred tank reactor.

In this study, we further investigate the performance of different reactor types in lab-scale yeast cultivations using *Pichia pastoris* yeast. It does not exhibit glucose repression of respiration and, therefore, is suitable for batch cultivation. Furthermore, its fermentative metabolism that produces mainly ethanol is activated at oxygen limitation (Baumann et al., 2008; Carnicer et al., 2009). Therefore, the presence of ethanol can be used as an indication of oxygen limitation even if

dissolved oxygen cannot be measured or if there are significant gradients, which may be the case especially in larger reactors. A kinetic model for the growth of *P. pastoris* on glucose, including the fermentative route in oxygen limited conditions and ethanol utilization, is formed based on chemostat cultivations presented in the literature. The model is qualitatively compared with batch cultivations in a laboratory-scale reactor. It is also applied in simulations along with a simple one-dimensional reactor scale model to assess the importance of scale-up effects – such as gas phase oxygen depletion, hydrostatic pressure, and liquid mixing – on oxygen transfer and cell yield during scale-up. The model is designed to be computationally light so that it can be applied also in the simulation of CFD-models developed for different reactors including the STDR, for example.

2 Materials and methods

Laboratory scale batch cultivations were carried out using *Pichia pastoris* X33 yeast in batch cultivations with two reactor types: OKTOP9000® and stirred tank reactor agitated with three Rushton turbines. The main geometrical parameters are presented in Figure 1, and more information of the reactors including gas dispersion and mass transfer performance can be found from Tervasmäki et al. (2016). For the cultivation experiments, inoculum was cultivated overnight in a liquid YPD-medium in baffled shake flasks (2 x 500 ml), and the bioreactor cultivations (Biostat C-DCU, Sartorius, Germany) were carried out in a basal salt medium supplied with 4.35 ml/l PTM_1 trace salts at a temperature of 30 °C (Table 1). The liquid volumes were 10 l (STR) and 12.5 l (OKTOP®), and the reactor diameter was 190 mm. Gas flow was set to 18 l/min (v_s = 0.011 m/s or 1.5 – 1.8 VVM), and the agitation rate was 450 rpm and 720 rpm for STR and OKTOP®, respectively. This corresponds to volumetric power consumption of about 500 W/m^3. Aqueous ammonium hydroxide (25%) was used to adjust the pH between 5 – 5.5; an antifoam agent (Antifoam 204, Sigma-Aldrich) was used to control the foam. Dissolved oxygen was measured from the lower (approx. 10 cm from bottom, Oxyferm FDA 120, Hamilton, Switzerland) and upper part of the reactor (approx. 10 cm from surface, Visiferm, Hamilton, Switzerland). Concentrations of oxygen, carbon dioxide and hydrocarbons were measured by Innova 1313 gas analyser (LumaSense, Denmark).

Manual samples were collected during fermentation to measure cell dry weight (CDW) and glucose, ethanol, acetate and glycerol concentrations. Cell dry weight was measured by transferring 2 ml of sample suspension into pre-weighed centrifuge tubes (triplicates), which were centrifuged, after which the remaining cell pellet was suspended in 0.9% NaCl, centrifuged again and dried for 24 hours at 60 °C before weighing. The standard deviation of the cell dry weight measurements were in general well below 5% of the measured value except for the initial measurements with very low cell concentrations. Glucose, ethanol, acetate and glycerol were measured by HPLC (Agilent 1200 series) equipped with ICSep ICE-Coregel 87H-column. 5 mM H_2SO_4 was used as a mobile phase with a flow rate of 0.6 ml/min and column temperature was controlled at 60 °C. The compounds were detected with a refractive index detector (RID). The gas analyser reacts to ethanol in off-gas, and a correlation was established between the raw data from the gas analyser and the measured ethanol concentration of the samples. Thus, the data from the gas analyser could be used as an online measurement for ethanol. The estimation of liquid phase ethanol concentration from the off-gas depends on evaporation of ethanol from liquid to the gas phase. The agitation and aeration were maintained constant in the above experiments so similar conditions for reaching the vapour-liquid equilibrium during the cultivation could be assumed, and a good correlation (R^2 = 0.99) was established between the ethanol concentration measured from liquid samples (HPLC) and off-gas signal. There was still some deviation, and an error margin of about 10% can be considered for the ethanol estimation from off-gas. At very low ethanol concentrations below 1 g/l, the error may be even more than 50% but accurate on-line monitoring of very low ethanol concentrations is not critical for the experiments in this study.

170 Table 1. Basal salt medium (BSM) and PTM_1 trace salts used in the reactor cultivations.

Basal Salt Medium			PTM_1 Trace Salts		
Phosphoric acid (85 %)	24.0	ml/l	Copper sulfate (pentahydrate)	6	g/l
Calcium sulfate	0.93	g/l	Sodium iodide	0.08	g/l
Potassium sulfate	18.2	g/l	Manganese sulfate (monohydrate)	3	g/l
Magnesium sulfate (heptahydrate)	14.9	g/l	Sodium molybdate (dihydrate)	0.2	g/l
Potassium hydroxide	4.13	g/l	Boric acid	0.02	g/l
Glucose	80	g/l	Cobalt chloride	0.5	g/l
			Zinc chloride	20	g/l
			Ferrous sulfate (heptahydrate)	65	g/l
			Biotin	0.2	g/l
			Sulfuric acid	5	ml/l

171

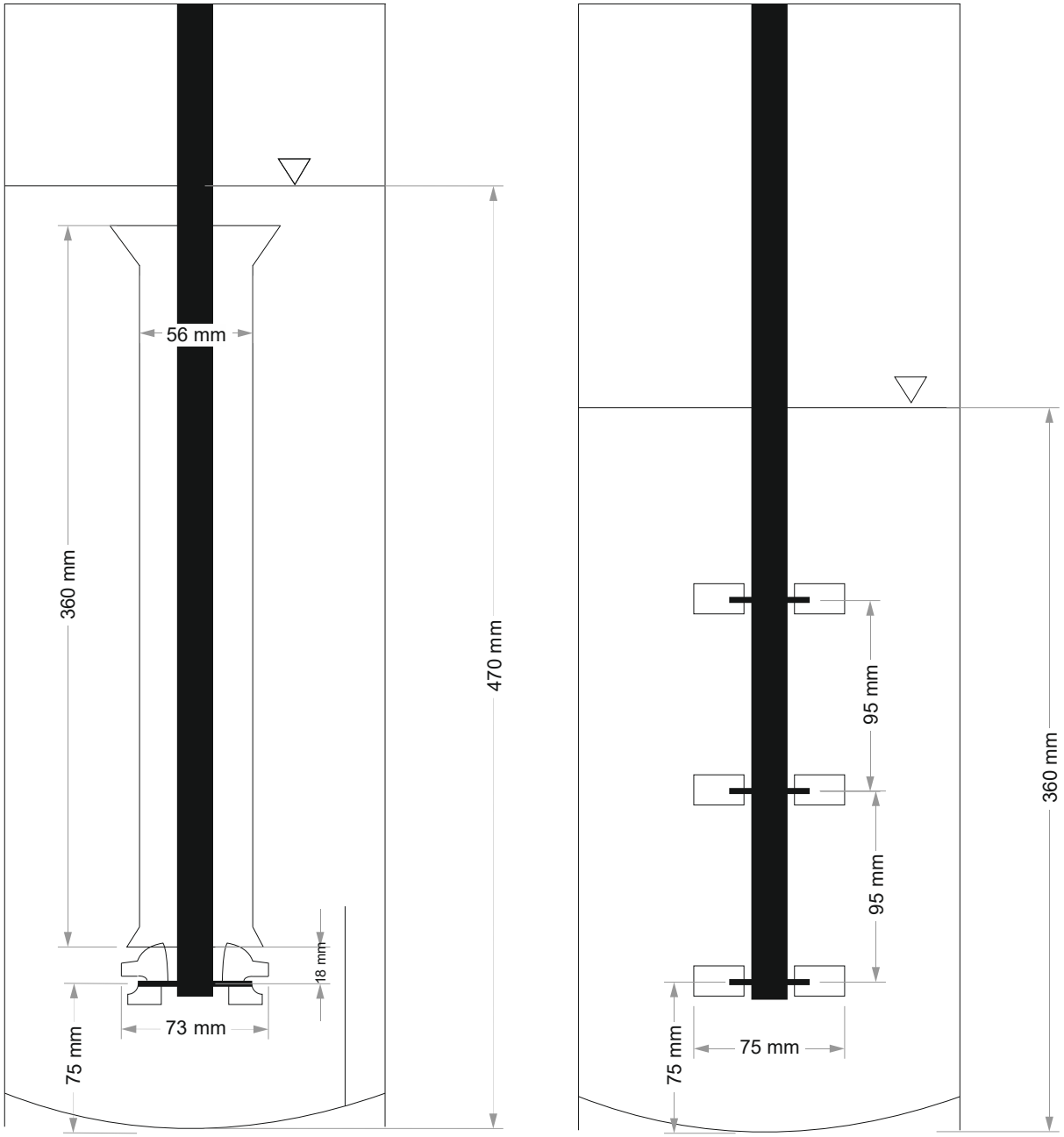

Figure 1. Reactor geometries for laboratory scale cultivations, OKTOP®9000 (left) and Rushton (right).

3 Modelling approach

3.1 Growth model for *Pichia pastoris*

The model is modified from the one presented by Sonnleitner and Käppeli (1986) for *Saccharomyces cerevisiae*. In the original model, specific glucose uptake is modelled using Monod kinetics with a

low value for saturation coefficient. If the glucose uptake rate exceeds the oxidative capacity of the cell, the rest of the glucose flux is directed towards fermentative metabolism producing ethanol thus capturing the glucose effect present in *S. cerevisiae* but not in *P. pastoris*. Therefore, the current model is modified so that the specific glucose uptake rate (q_g) is dependent on the growth rate and it is assumed that the oxidative capacity of the cells exceeds the oxygen requirement even at the maximum growth rate, given that oxygen transfer rate of the reactor is sufficient to maintain dissolved oxygen above a critical level. In addition, ethanol can also be utilized as a carbon source if oxygen is available and glucose is not present in the medium. The net stoichiometric equations of the three metabolic routes are as follows:

$C_6H_{12}O_6 + aO_2 + bNX[NH_3] \rightarrow bCH_{HX}O_{OX}N_{NX} + cCO_2 + dH_2O$ (glucose oxidation)

$C_6H_{12}O_6 + gNX[NH_3] \rightarrow gCH_{HX}O_{OX}N_{NX} + hCO_2 + iH_2O + jC_2H_6O$ (glucose fermentation)

$C_2H_6O + kO_2 + lNX[NH_3] \rightarrow lCH_{HX}O_{OX}N_{NX} + mCO_2 + nH_2O$ (ethanol oxidation)

Stoichiometric coefficients *b*, *g* and *l* can be derived directly from biomass yield coefficients for glucose oxidation, glucose fermentation and ethanol oxidation (Y_{xg}^{ox}, $Y_{xg}^{ferm}$and Y_{xe}^{ox}, see Table 2) and molecular weights of biomass, glucose and ethanol. Coefficients for the molar composition of cell mass, *HX, OX* and *NX* are derived from Carnicer et al. (2009). This leaves three unknown coefficients and three elemental balance equations (C, H, O) for each stoichiometric equation, from which yield coefficients ($Y_{og}^{ox} = 0.43\frac{g_{O2}}{g_{glu}}$, $Y_{eg}^{ferm} = 0.48\frac{g_e}{g_{glu}}$ and $Y_{oe}^{ox} = 1.88\frac{g_{O2}}{g_e}$) can be solved.

The model equations are presented below. In brief, the model consists of equations for the specific uptake rate of glucose by oxidative (1) or fermentative (2) metabolism and ethanol by oxidative metabolism (3) by Monod-type equations including also the effect of dissolved oxygen concentration for oxidative metabolism and glucose inhibition of ethanol consumption. The corresponding specific growth rates (4) – (6), and oxygen consumption from oxidation of glucose and ethanol (7) – (8) are calculated using the yield coefficients. Mass balance equations for glucose, ethanol, cell mass and dissolved oxygen concentrations are presented in equations (9) – (11).

$$q_{\mathrm{g}}^{\mathrm{ox}} = \frac{\mu_{\mathrm{max}}^{\mathrm{ox}}}{Y_{\mathrm{xg}}^{\mathrm{ox}}} \frac{c_{\mathrm{g}}}{c_{\mathrm{g}} + K_{\mathrm{g}}} \frac{c_{\mathrm{o}}}{c_{\mathrm{o}} + K_{\mathrm{o}}} \quad (1)$$

$$q_{\mathrm{g}}^{\mathrm{ferm}} = \frac{\mu_{\mathrm{max}}^{\mathrm{ferm}}}{Y_{\mathrm{xg}}^{\mathrm{ferm}}} \frac{c_{\mathrm{g}}}{c_{\mathrm{g}} + K_{\mathrm{g}}} \left(1 - \frac{c_{\mathrm{o}}}{c_{\mathrm{o}} + K_{\mathrm{o}}}\right) \quad (2)$$

$$q_{\mathrm{e}}^{\mathrm{ox}} = \frac{\mu_{\mathrm{max}}^{\mathrm{e}}}{Y_{\mathrm{xe}}^{\mathrm{ox}}} \frac{c_{\mathrm{e}}}{c_{\mathrm{e}} + K_{\mathrm{e}}} \frac{K_{\mathrm{i}}}{c_{\mathrm{g}} + K_{\mathrm{i}}} \frac{c_{\mathrm{o}}}{c_{\mathrm{o}} + K_{\mathrm{o}}} \quad (3)$$

$$\mu_{\mathrm{g}}^{\mathrm{ox}} = q_{\mathrm{g}}^{\mathrm{ox}} Y_{\mathrm{xg}}^{\mathrm{ox}} \quad (4)$$

$$\mu_{\mathrm{g}}^{\mathrm{ferm}} = q_{\mathrm{g}}^{\mathrm{ferm}} Y_{\mathrm{xg}}^{\mathrm{ferm}} \quad (5)$$

$$\mu_{\mathrm{e}}^{\mathrm{ox}} = q_{\mathrm{e}}^{\mathrm{ox}} Y_{\mathrm{xe}}^{\mathrm{ox}} \quad (6)$$

$$q_{\mathrm{o}}^{\mathrm{g}} = q_{\mathrm{g}}^{\mathrm{ox}} Y_{\mathrm{og}}^{\mathrm{ox}} \quad (7)$$

$$q_{\mathrm{o}}^{\mathrm{e}} = q_{\mathrm{e}}^{\mathrm{ox}} Y_{\mathrm{oe}}^{\mathrm{ox}} \quad (8)$$

$$\frac{dc_i}{dt} = \frac{F_{\mathrm{in}}}{V} c_{i,\mathrm{in}} - \frac{F_{\mathrm{out}}}{V} c_i - \left(q_i^{\mathrm{ox}} + q_i^{\mathrm{ferm}}\right) c_{\mathrm{x}} \quad (9)$$

$$\frac{dc_{\mathrm{x}}}{dt} = \frac{F_{\mathrm{in}}}{V} c_{\mathrm{x,in}} - \frac{F_{\mathrm{out}}}{V} c_{\mathrm{x}} - \left(\mu_{\mathrm{g}}^{\mathrm{ox}} + \mu_{\mathrm{g}}^{\mathrm{ferm}} + \mu_{\mathrm{e}}^{\mathrm{ox}}\right) c_{\mathrm{x}} \quad (10)$$

$$\frac{dc_{\mathrm{o}}}{dt} = k_{\mathrm{L}} a (c_{\mathrm{o}}^{\mathrm{sat}} - c_{\mathrm{o}}) - (q_{\mathrm{o}}^{\mathrm{g}} + q_{\mathrm{o}}^{\mathrm{e}}) c_{\mathrm{x}} \quad (11)$$

$$c_{\mathrm{o}}^{\mathrm{sat}} = \frac{p_{\mathrm{o}}}{k_{\mathrm{H}}} \quad (12)$$

Where q_i is specific rate of component *i* ($g_i\ g_x^{-1}\ h^{-1}$) and x, g, e and o denote cells, glucose, ethanol and oxygen, respectively. Parameters μ_{max}, *Y* and *K* are listed in Table 2, c_i is concentration of component *i* (g/l), *F* is flow rate (l/h) and *V* is liquid volume (l). For continuous cultivations $F_{in} = F_{out} = F$, and dilution rate $D = F/V$. c_o^{sat} is the saturation concentration of oxygen in liquid, p_o is the partial pressure of oxygen in the gas phase and k_H is Henry's constant for oxygen in water.

209 Table 2. Parameters used in the growth model of Pichia pastoris

Parameter	Dimension	Value	Reference
$\mu_{\max}^{\mathrm{ox}}$	h^{-1}	0.18	Solà et al. (2004)
$\mu_{\max}^{\mathrm{ferm}}$	h^{-1}	0.058	This work, adjusted
$\mu_{\max}^{\mathrm{e}}$	h^{-1}	0.15	This work, adjusted
$Y_{\mathrm{xg}}^{\mathrm{ox}}$	$g_{cells}\ g_{glu}^{-1}$	0.49	Sonnleitner and Käppeli (1986)
$Y_{\mathrm{xg}}^{\mathrm{ferm}}$	$g_{cells}\ g_{glu}^{-1}$	0.05	Sonnleitner and Käppeli (1986)
$Y_{\mathrm{xe}}^{\mathrm{ox}}$	$g_{cells}\ g_{etoh}^{-1}$	0.57	Sonnleitner and Käppeli (1986)
K_{g}	$g_{glu}\ l^{-1}$	0.1	Sonnleitner and Käppeli (1986)
K_{o}	$mg_{O2}\ l^{-1}$	0.109	This work, adjusted
K_{e}	$g_{etoh}\ l^{-1}$	0.1	Sonnleitner and Käppeli (1986)
K_i	$g_{glu}\ l^{-1}$	0.1	Sonnleitner and Käppeli (1986)
HX	$mol_H\ mol_C^{-1}$	1.69	Carnicer et al. (2009)
OX	$mol_O\ mol_C^{-1}$	0.592	Carnicer et al. (2009)
NX	$mol_N\ mol_C^{-1}$	0.139	Carnicer et al. (2009)

210

211 Literature data from continuous cultivations were used to determine model parameters either
212 directly or by fitting the model to the data. Literature experiments included in this study were
213 conducted with dilution rates between 0.1 – 0.16 h^{-1}, inlet glucose concentration between 8 – 50
214 g/l, and inlet gas with varying oxygen content ranging from 5.9% to 21% (Baumann et al., 2008,
215 2010; Carnicer et al., 2012; Solà et al., 2004). A total of 11 experiments were included, and the
216 responses used for parameter estimation were steady state concentrations for ethanol and cell
217 mass, which were either directly reported in the references or estimated from the reported specific
218 rates (see Table 3). In addition, relative k_La-values for the reactors were estimated based on the
219 stirrer speed, gas flow and reactor geometry reported in the references. An additional coefficient to
220 scale the dimensionless k_La was estimated along with the growth parameters.

221

Table 3. Experimental setup in the literature references. Relative mass transfer coefficient values are estimated based on the reported reactor geometry and operational conditions (agitation, aeration). Steady state concentration of cell mass and glucose are calculated from the reported specific rates if not directly given in the reference (*).

	k_La (relative)	O_2 in gas	D	$c_{glu,in}$	c_x	c_e
	-	%	h-1	g/l	g/l	g/l
(Carnicer et al., 2012)	0.2	21	0.10	8	3.86*	0*
	0.2	11	0.10	8	3.05*	0.43*
	0.2	8	0.10	8	2.28*	0.88*
(Solà et al., 2004)	0.4	21	0.16	10	5.42*	0
(Baumann et al., 2010)	1	21	0.10	50	23.98	0
	1	11	0.10	50	22.54	0.89
	1	8	0.10	50	12.58	6.85
(Baumann et al., 2008)	1	21	0.10	50	23.97	0.25
	1	11	0.10	50	22.56	0.68
	1	8.4	0.10	50	12.96	5.61
	1	5.9	0.10	50	12.03	5.78

3.2 Reactor model

The growth model presented in the previous section assumed perfect mixing of gas and liquid phases and no depletion of the oxygen in gas phase. Laboratory scale cultivations are usually carried out at a relatively high gas flow rate when calculated per volume of liquid phase (VVM). Therefore, the gas phase residence time is short, and depletion of oxygen from the gas phase can often be ignored. However, if the gas flow rate is scaled up by using a superficial gas flow rate (v_s, m/s), the VVM-value decreases during scale-up, particularly for tall vessels with a high aspect ratio (Nauha et al., 2015). Thus, gas phase residence time increases and gas phase depletion may become significant. In addition, hydrostatic pressure may be significant in tall vessels adding approximately one bar for every 10 m of liquid height. This, on the other hand, increases the driving force for mass transfer described in equation (12). Also, the distribution of agitation power, affecting mass transfer characteristics, such as liquid side mass transfer coefficient (k_L), bubble size (d_b), and gas hold-up (ϕ) is uneven and the gradients increase with scale.

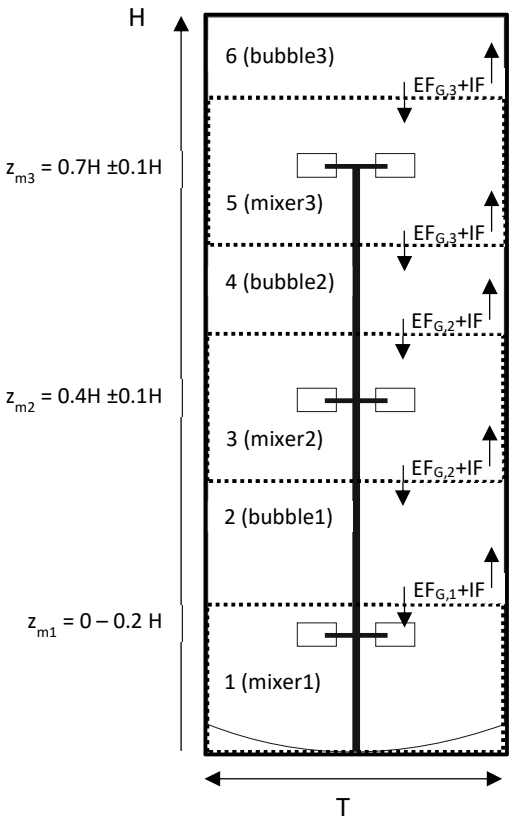

Figure 2. Schematic presentation of reactor scale model. The reactor is divided to three mixer and three bubble compartments, a total of six zones (*j*). Mass transfer coefficient and gas hold-up are estimated separately for each zone by equations (13)-(18), and the flow between compartments (EF_G + IF) is calculated by equations (21)-(22).

In the reactor scale model, the reactor is divided into six zones – three mixer zones and three bubble zones between the impellers (Figure 2). Thus, it is applicable for STR with three impellers, and the zones around and between the impellers can be expressed separately. For mixer zones (*j* = 1, 3, 5), mass transfer and gas hold-up values are calculated based on volumetric power input and superficial gas velocity (equations (13) – (16)), whereas for bubble zones (*j* = 2, 4, 6) the values are calculated based on superficial gas velocity only (equations (17) – (18)). The mixer zone values are estimated as follows. Liquid side mass transfer coefficient k_L, mass-transfer area *a* and bubble diameter d_b in the homogeneous regime are estimated from equations in Nauha et al. (2015, eq22, 13 and 21) and hold-up ϕ from equation in Vrábel et al. (2000, eq17).

$$k_{L,j} = 0.301\sqrt{D_L}\left(\frac{\left(\frac{P}{V}\right)_j}{\eta_{liq}}\right)^{0.25} \quad (13)$$

$$a_j = \frac{6\phi_j}{d_{\mathrm{b},j}} \quad (14)$$

$$d_{\mathrm{b},j} = 0.7\frac{\sigma^{0.6}}{(P/V)_j^{0.4}\rho_{\mathrm{l}}^{0.2}}\left(\frac{\eta_{\mathrm{liq}}}{\eta_{\mathrm{gas}}}\right)^{0.1} \quad (15)$$

$$\phi_j = 0.37(P/V)_j^{0.16}v_{\mathrm{s}}^{0.55} \quad (16)$$

where D_{L} is the diffusion coefficient for oxygen in water (1.97e-9 m^2 s^{-1}) and η is viscosity (Pa s). The effect of mixer power input on gas hold-up in the large (> 10 m^3) scale is much lower compared to the laboratory scale (< 100 l), and the exponent on (P/V) can be over 0.3 on the laboratory scale compared to 0.16 used in the present calculations (Vrábel et al., 2000). For the area between mixers—the so-called bubble region—hold-up is estimated from Nauha et al. (2015, eq11) and $k_{\mathrm{L}}a$ from Oosterhuis and Kossen (1984, eq4).

$$\phi_j = \frac{v_{\mathrm{s}}}{U_{\mathrm{T}}} \quad (17)$$

$$k_{\mathrm{L}}a_j = 0.3v_{\mathrm{s}}^{0.7} \quad (18)$$

U_{T} is the terminal velocity of the bubbles, which is assumed to be constant (0.2 m s^{-1}, Nauha et al., 2015). However, if the hold-up or $k_{\mathrm{L}}a$ estimated from the mixer zone equations is lower compared to the bubble zone, the bubble zone values are also used for the (particular) mixer zone. When calculating the mass transfer rate in the compartment i, $k_{\mathrm{L}}a_{\mathrm{i}}(C_{\mathrm{o,i}}^{\mathrm{sat}} - C_{\mathrm{o}})$, the value for $C_{\mathrm{o,i}}^{\mathrm{sat}}$ is affected by the partial pressure of oxygen in the gas phase. The residence time of the gas phase in compartment i (τ_{i}) is dependent on the gas volume in the compartment and the volumetric gas flow rate (F_{gas}).

$$c_{\mathrm{o},j}^{\mathrm{sat}} = \frac{y_{\mathrm{o,gas},j}\left(P_{\mathrm{h}} + \rho g(H - z_j)\right)}{k_{\mathrm{H}}} \quad (19)$$

$$\tau_j = \frac{V_j\phi_j}{F_{gas}} \quad (20)$$

The effect of liquid mixing was estimated by compartment modelling approach. The model presented here is simplified from the one presented in (Vrábel et al., 2000) and it is one dimensional accounting for the axial dimension. Thus, circulation flow within the compartments around each stirrer and between stirrers are omitted, and the model consists of exchange flow in gassed conditions (EF_G) and induced flow (IF) between the compartments as shown in Figure 2. For the Rushton turbine geometry:

$$EF_G = 0.34\alpha T^2 D^{1/3}(1-\varepsilon)\left[\frac{(P_G/P)N_P N^3 D^5}{0.25\pi T^2 H_i(1-\varepsilon)}\right] \quad (21)$$

$$IF = 0.07A_{gap}[1-(D/T)^2]^{-4.75}\frac{Q_g}{\left(\frac{P_g}{P}\right)^{\beta} ND^3} \quad (22)$$

where α = 0.07 m/s and β = 0.3 are model parameters, A_{gap} is the area of the gap between vessel wall and impeller sweep area, and H_i is the height of the impeller region (Figure 2). The mass balance equations (9)-(11) were modified to include the flow between the compartments (EF_G + IF), and local values for mass transfer coefficient and gas hold-up. In addition the gas phase oxygen content (23) was included, and the saturation concentration for oxygen in liquid was calculated based on the hydrostatic pressure and gas phase oxygen content.

$$\frac{dc_{\mathrm{o,gas},j}}{dt} = \frac{c_{\mathrm{o,gas,j-1}} - c_{\mathrm{o,gas},j}}{\tau_j} - \frac{k_{\mathrm{L}}a_j}{\phi_j}\left(c_{\mathrm{o},j}^{\mathrm{sat}} - c_{\mathrm{o}}\right) \quad (23)$$

Where $c_{\mathrm{o,gas,j}}$ is the oxygen concentration in the gas phase of compartment *j* and *j* = 0 for the inlet gas.

4 Results and discussion

4.1 Yeast cultivations

The yeast cultivations were carried out with a constant stirrer speed and gas flow rate, which resulted in low dissolved oxygen concentrations during growth on glucose in both reactors (Figure 3). Thus, significant amounts of ethanol were produced in both cultivations towards the end of the glucose phase, which lasted about 21 h. The peak ethanol concentrations before ethanol consumption phase were 14.6 and 12.5 g/l for Rushton and OKTOP®-geometries, respectively. The

lower ethanol concentration in the OKTOP® reactor is likely due to a higher dissolved oxygen concentration. Although DO drops to about 2% at the lower probe in both reactors, it reaches such a low value already at 15 h in the STR, whereas the limit of 2% is reached only after 20 h in the OKTOP® reactor. Also, DO at the probe positioned in the upper part of the reactor was higher in OKTOP® (approx. 20% vs. 10%). After glucose consumption, there is a short lag-phase before ethanol consumption, and the fermentations were finished at about 35 h. The cell concentrations after the glucose phase were 18.5 g/l and 19.6 g/l and after ethanol consumption 26.8 g/l and 29.5 g/l for STR and OKTOP®, respectively. Thus, the peak ethanol concentration was lower and final cell concentration was higher in the cultivation carried out in the OKTOP® reactor.

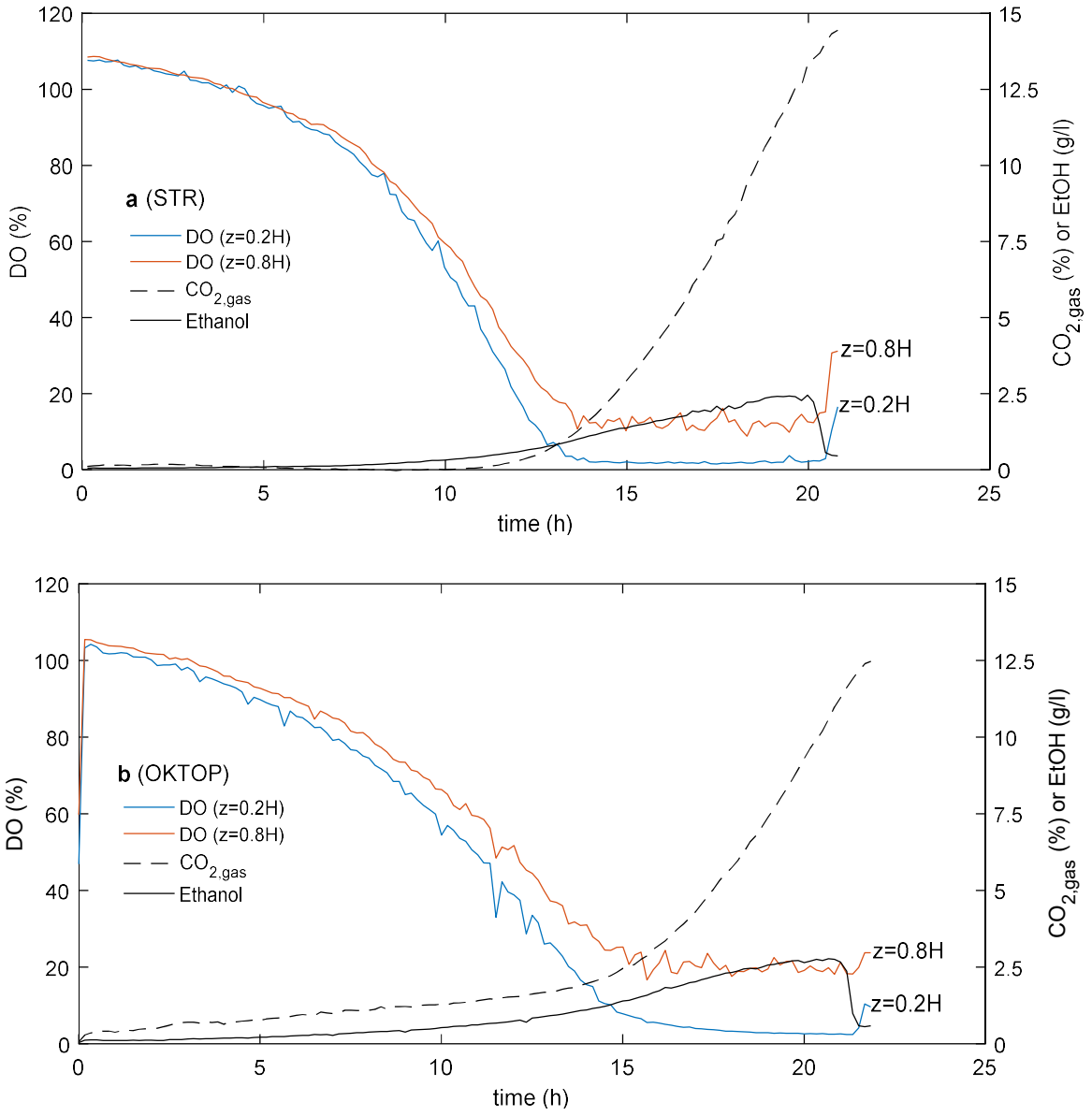

Figure 3. Measurement data from lab-scale cultivations **a)** Stirred tank reactor agitated with three Rushton turbines **b)** OKTOP® reactor

4.2 Growth model for *Pichia pastoris*

The model parameters were mainly from literature sources, and they are listed in Table 2. Three parameters, μ_{max}^{ferm} (maximum specific growth rate on glucose via fermentation), μ_{max}^{e} (maximum specific growth rate on glucose via fermentation) and K_o (saturation coefficient for oxygen uptake) were estimated using data from chemostat cultivations presented in the literature in different cultivation conditions (Table 3, Baumann et al., 2008, 2010; Carnicer et al., 2012; Solà et al., 2004).

306 An example of the effect of inlet gas oxygen concentration is presented in Figure 4a. It can be seen
307 that in the investigated conditions, ethanol production is negligible when oxygen content of the
308 inlet gas is above 10%, and cell concentration is above 20 g/l, both of which are well predicted by
309 the model. At lower inlet gas oxygen concentrations, ethanol is produced and cell concentration
310 decreases. The model qualitatively captures the effect, although there is some deviation between
311 the data in the literature references and the model prediction. Parity plot for all experimental points
312 of steady state cell mass and ethanol concentration is presented in Figure 4b and correspondence
313 between the model and experimental data is quite good.

314 The model was also applied to the batch cultivation in STR discussed in section 4.1. The initial
315 conditions were the same as in the batch experiment and k_La was estimated to be 250 h^{-1} in the
316 experimental conditions based on previous research (Tervasmäki et al., 2016). A lag time of one
317 hour was manually adjusted for the model prediction so that the time of glucose exhaustion is
318 roughly the same as in the experiments. The results are presented in Figure 5 for glucose, ethanol,
319 and cell mass concentrations (a), as well as for dissolved oxygen (b). The model corresponds quite
320 well with the cultivation conditions. Only the cell concentrations after the glucose consumption
321 phase are significantly over predicted, and the final cell concentration is overestimated by almost
322 30%. There is also a possibility that higher amounts of ethanol were produced than the measured
323 concentrations that as part of the ethanol escaped with the exhaust gas thus not accumulating in
324 the liquid. Therefore, the difference between the measured and estimated cell concentrations could
325 be due to higher peak ethanol concentration, which would lower the cell yield from glucose.
326 However, the model qualitatively captures the decrease in growth rate after switching the carbon
327 source from glucose to ethanol.

328 In addition, the dissolved oxygen concentration during the cultivation follows the same trend as the
329 measured values. The model fails to capture the short peak at 21 h indicating the switch in
330 metabolism from glucose to ethanol utilization. This is expected, as detailed metabolic routes were
331 not included in the model. Structured modelling approaches such as cybernetic modelling (Ho et al.,
332 2015; Ramkrishna and Song, 2012), genome-scale models (GEMs) or structured kinetic models
333 (Heijnen, 2005; Kerkhoven et al., 2015) may enable more rigorous description of the observed

phenomena. However, the goal here is to describe a model with low computational load to be applied in bioreactor simulations. The short increase in the measured dissolved oxygen concentration between 28 and 31 h was due to a temporary increase in the agitation rate, and the model results were calculated with a constant k_La value. Based on the discussion above, it can be concluded that the model is also adequate for estimating batch culture behaviour.

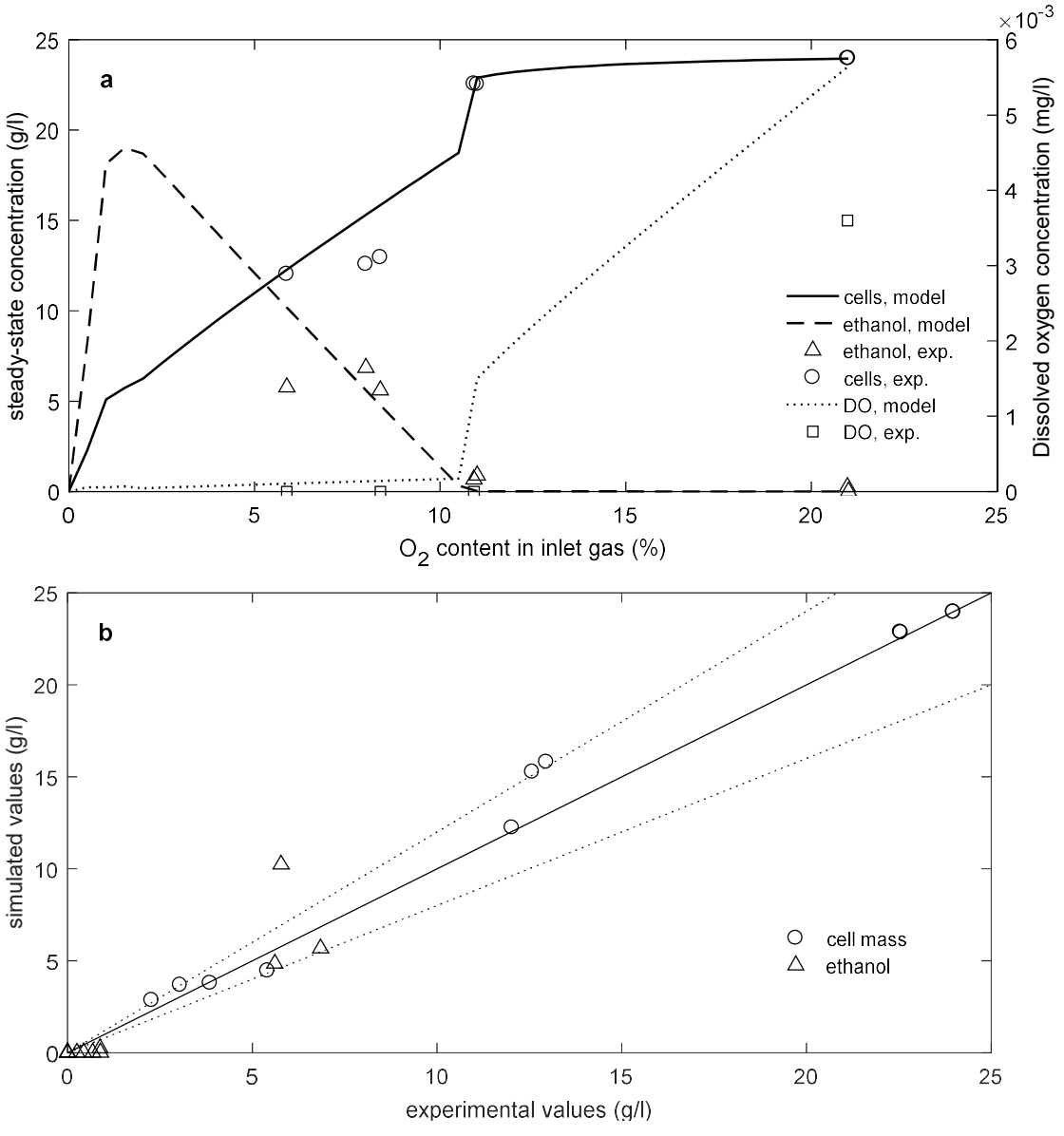

Figure 4. **a)** Steady-state concentration of cell mass and ethanol (experimental and simulated) and dissolved oxygen (simulated) vs. the oxygen content of inlet gas for $c_{g,in}$ = 50 g/l and D = 0.1 h-1 as reported in (Baumann et al., 2008, 2010). **b)** Simulated and experimental values for steady-state concentration of cell mass and ethanol in all chemostat cultivation conditions in the literature, dotted lines show +/- 20% margin.

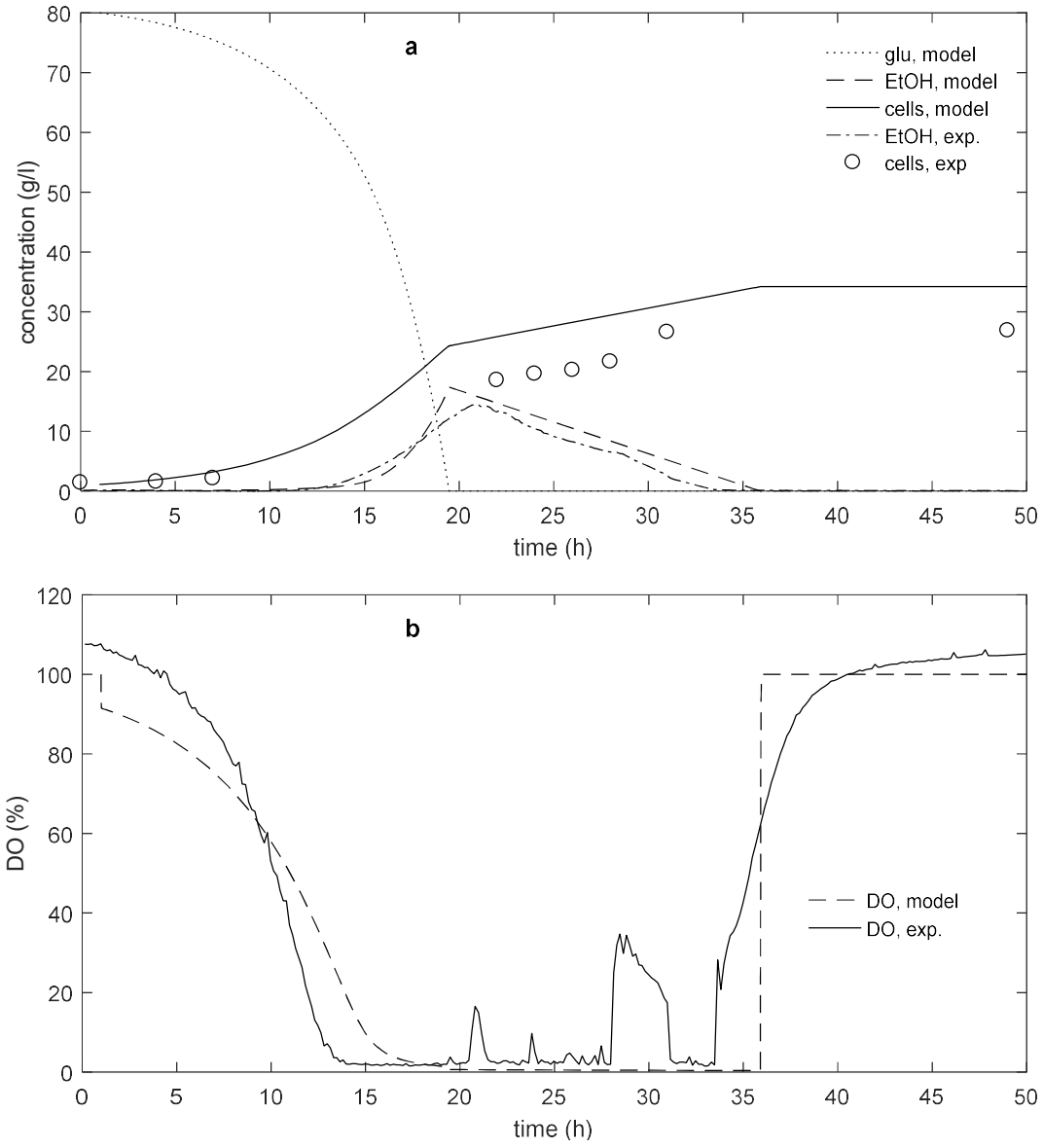

Figure 5. Comparison of model prediction to batch cultivation data in STR, additional lag time of one hour was added to the model prediction. Estimated k_La for the simulations was 250 h^{-1} **a)** glucose, ethanol and cell concentration **b)** dissolved oxygen

One way to study the effect of oxygen transfer on culture conditions using the model is by plotting the steady-state cell mass, glucose and ethanol concentrations of a continuous cultivation as a function of dilution rate D. This has been done in Figure 6a for two k_La-values (250 h^{-1} and 500 h^{-1}). It can be seen that for lower k_La, the steady-state cell concentration begins to decrease when D > 0.07 h^{-1} and it can be explained by oxygen limitation with simultaneously occurring ethanol accumulation. When the dilution rate is further increased above 0.15 h^{-1}, culture washout occurs.

In the simulation with higher mass transfer coefficient, there is very little variation in cell concentrations with $D < 0.16$ h^{-1}, and culture washout occurs sharply at $D > 0.17$ h^{-1}. This value is close to the maximum growth rate and this type of behaviour is typical for ideal continuous cultivation. Thus, oxygen limitation can be detected from decreased cell yield, ethanol accumulation, and washout at a lower dilution rate due to decreased growth rate.

The effect of k_La is further elucidated in Figure 6b, in which steady-state concentrations (cells, glucose, ethanol, dissolved oxygen) are plotted with respect to k_La at $D = 0.1$ h^{-1}. It can be seen that the conditions are mass transfer limited when $k_La < 400$ h^{-1}, which can be seen as low dissolved oxygen concentration and accumulation of ethanol. Increasing the mass transfer rate further increases the dissolved oxygen concentration, but has no effects on cell concentration if the critical value is exceeded. This is a very similar situation to the one presented for the data in the literature in Figure 4 for inlet gas oxygen concentration as both parameters (k_La and gas composition) directly affect the oxygen transfer rate.

The model sensitivity to parameters was assessed by calculating the relative change in glucose, ethanol, cell, and dissolved oxygen concentrations when each parameter was increased by 10% from the values presented in Table 2. The results are presented in Figure 7 in which the sensitivities are plotted as heat maps with $c_{glu,in} = 40$ g/l, $D = 0.1$ h^{-1} (a-b) or $D = 0.15$ h^{-1} (c-d), and $k_La = 250$ h^{-1} (a, c) or $k_La = 500$ h^{-1} (b, d). The concentrations calculated with the optimal parameters can be seen in Figure 6.

The model shows less sensitivity for the lower dilution rate, which can be expected when looking at the data in Figure 6a. The cell washout occurs at dilution rates between 0.15 – 0.17 h^{-1}, and the parameter sensitivity is increased at that in that range. It should be noted that some of the seemingly high sensitivity values are due to very low concentrations calculated with the optimal parameters. For example, the ethanol concentrations with higher k_La-value (500 h^{-1}) are below 0.06 g/l so even minor changes in the absolute concentration affect the relative values (Figure 7b). Same applies for glucose although the concentrations are slightly higher between 0.1 – 0.5 g/l. The effect of parameters describing the elemental composition of the cells (*OX*, *HX* and *NX*) have similar effect

as the yield parameters. However, the elemental composition is expected to vary less than 10% (Carnicer et al., 2009).

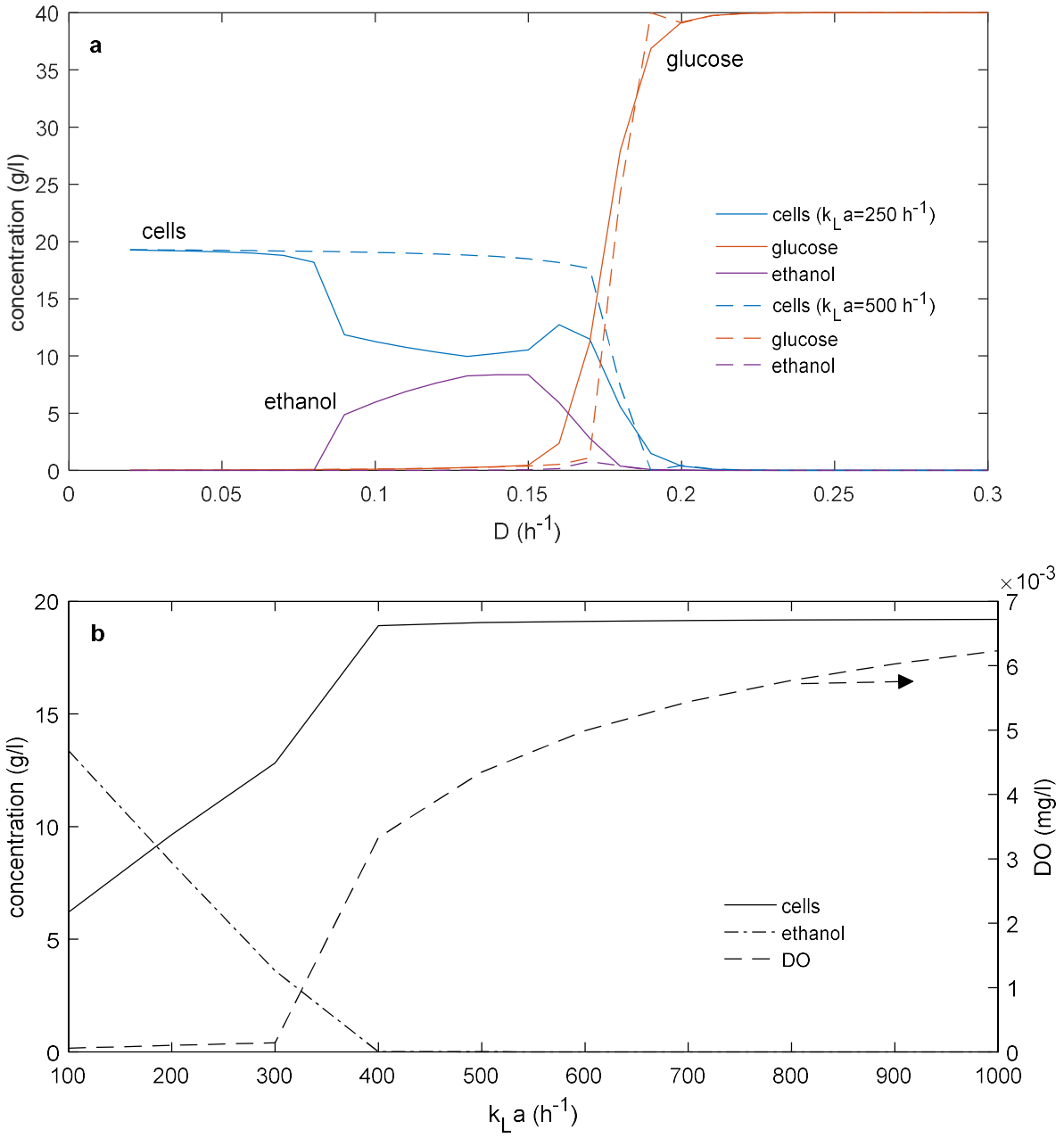

Figure 6. Steady-state concentrations for chemostat simulations with $c_{glu,in}$ = 40 g/l. **a)** cells, glucose and ethanol as a function of dilution rate with k_La = 250 and 500 h^{-1} **b)** cells, ethanol and dissolved oxygen as a function of k_La with D = 0.1 h^{-1}

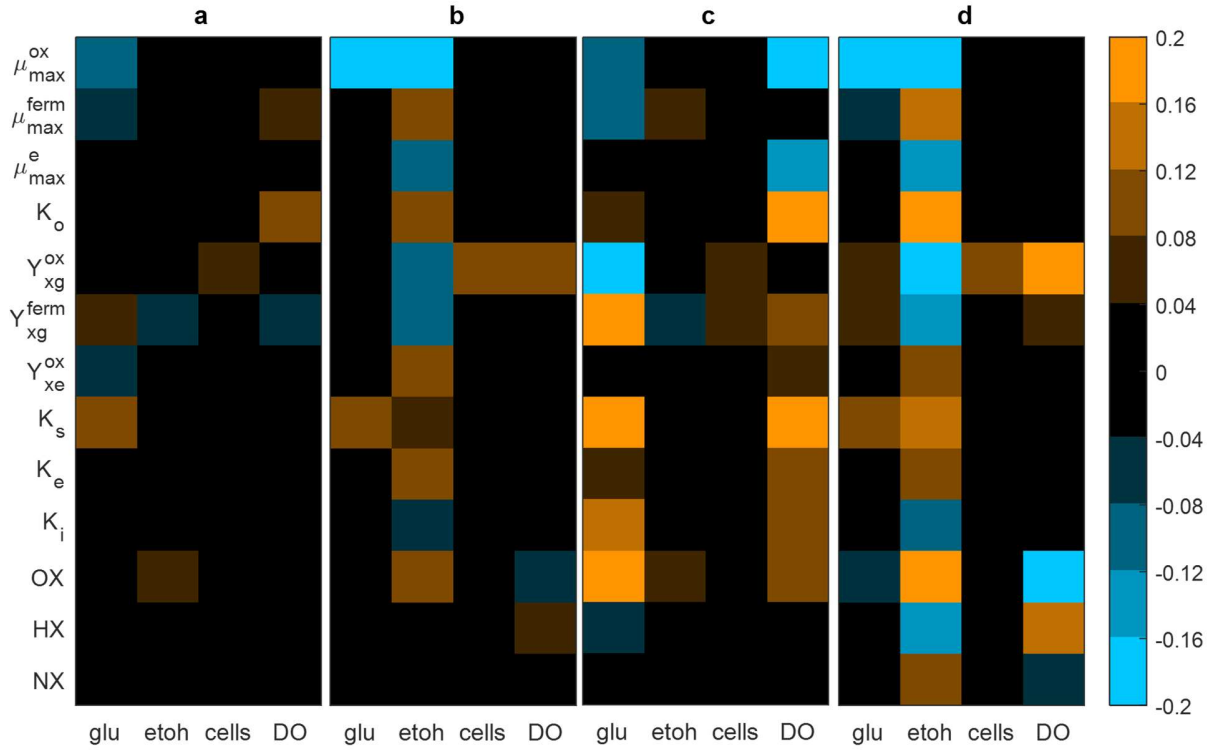

Figure 7. Parameter sensitivity of model-predicted glucose, ethanol, cell and dissolved oxygen concentrations in steady-state of chemostat operation with $c_{glu,in}$ = 40 g/l. Relative change of concentrations when each parameter was increased by 10%. **a)** D = 0.1 h^{-1} and k_La = 250 h^{-1} **b)** D = 0.1 h^{-1} and k_La = 500 h^{-1} **c)** D = 0.15 h^{-1} and k_La = 250 h^{-1} **d)** D = 0.15 h^{-1} and k_La = 500 h^{-1}

4.3 Scale-up effects

The simulations to study scale-up effects were made at similar conditions as in Figure 6 (D = 0.1 h^{-1} and $c_{glu,in}$ = 40 g/l), and the aspect ratio was fixed to H/T = 3. Maximum gas flow was maintained at v_s = 0.03 m/s so that a homogeneous flow regime could be assumed, which is a prerequisite for equations (13(18). The volumetric power consumption between 250 – 1000 W/m^3 was used in the simulations. The main factor that affects the cell growth in reactors of different scale and operational conditions in the investigated domain is the dissolved oxygen concentration. The effect of scale and operational conditions on dissolved oxygen and oxygen transfer conditions are shown in Figure 8 in which dimensionless axial profiles of dissolved oxygen are plotted for 10 and 1000 m^3 reactors with different agitation and aeration rates. In addition, the dimensionless profiles of oxygen saturation concentration, taking into account hydrostatic pressure and oxygen content of the gas phase are included in the plots to illustrate the driving force for mass transfer.

In the smaller reactor (10 m^3, a,b,e,f), the dissolved oxygen concentration is quite uniform, and increasing the agitation from 250 to 1000 W/m^3 (b,f) would be sufficient to increase the dissolved oxygen level and prevent fermentative metabolism due to oxygen limitation. The profile showing the saturation concentration of oxygen is also quite uniform as depletion of oxygen and hydrostatic pressure effects are insignificant. In larger reactor (1000 m^3, c, d, g, h), however, the dissolved oxygen and saturation curves are more curved, and values are lower at the upper part of the reactor. This is due to oxygen depletion of gas phase and hydrostatic pressure effects, which both affect the driving force for mass transfer. Another factor is insufficient mixing in the axial direction of the dispersion allowing significant gradients for oxygen. The effect of scale is more profound when the superficial gas velocity is lower, and increasing the agitation power in the large scale is not sufficient to overcome these effects.

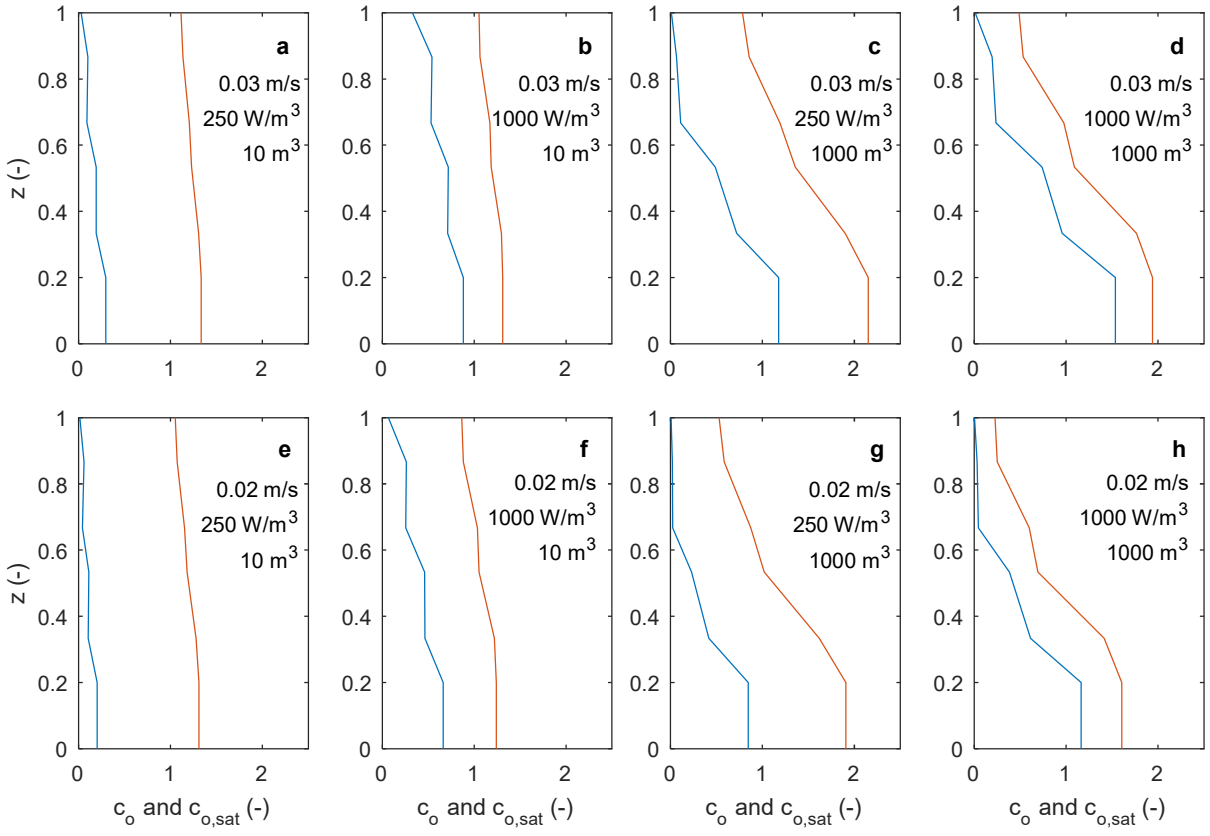

Figure 8. Dimensionless axial profile of dissolved oxygen (blue line, c_o) and saturation concentration (red line, $c_{o,sat}$ calculated based on hydrostatic pressure and gas phase oxygen fraction) in STR. Corresponding cell yield is shown in Figure 9.

A more general view of the effect of reactor volume and operational conditions on simulated steady-state conditions can be seen in Figure 9 in which the steady-state concentrations of cells are plotted against the reactor volume. The cell concentrations are scaled by the theoretical maximum values so that fully aerobic metabolism with highest cell yield would give a value of one. Three overall volumetric power inputs (250, 500 and 1000 W/m^3) and two superficial gas velocities (0.02 m/s and 0.03 m/s) are included. The conditions for which axial profiles of oxygen are plotted in Figure 8 are shown in circles. It can be seen that in small reactors with the highest gas flow and power input (volume averaged k_La = 427 h^{-1}), the cell yield is almost at its maximum, a similar situation to that in Figure 6b with k_La > 400 h^{-1}. With increasing scale, however, the cell yield decreases as the dissolved oxygen decreases although the overall k_La remains constant. The decrease in cell yield is mainly due to increased gas phase residence time and oxygen depletion, and the variation of dissolved oxygen concentration along the reactor. It is more profound when superficial gas velocity is lower. It can also be noted that the effect of power input decreases with scale as the curves with different power inputs approach each other. Therefore, increasing the agitation power yields only a minor improvement.

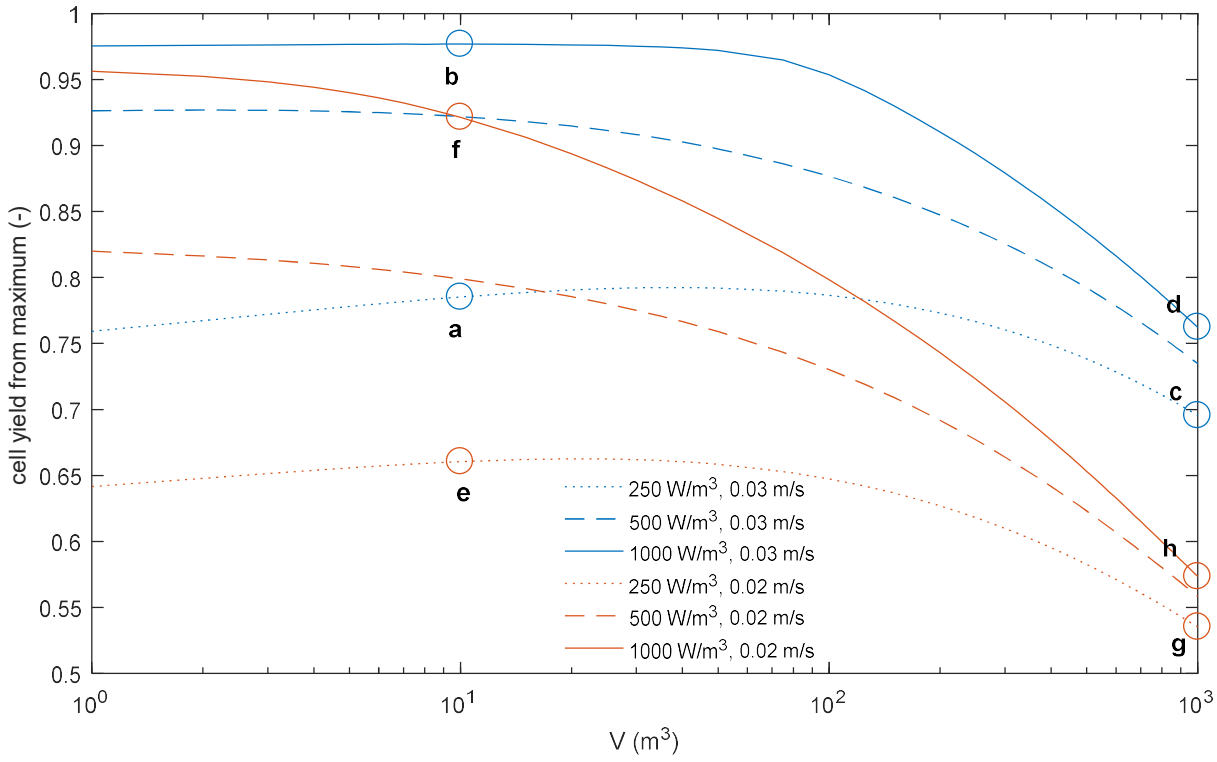

Figure 9. The effect of reactor scale (STR), gas flow and agitation power on chemostat steady state, simulations were run with, D = 0.1 h^{-1}, H/T = 3, $c_{glu,in}$ = 40 g/l. The steady-state cell concentration is scaled with theoretical maximum values for v_s = 0.03 m/s, overall k_La-values 164, 260 and 427 h^{-1} for increasing power input and for v_s = 0.02 m/s, overall k_La-values 130, 206 and 340 h^{-1} for increasing power input. Letters a-g mark the examples shown in Figure 8 for the axial profile of oxygen

Insufficient mixing of the bulk dispersion also causes detrimental effects in the large-scale simulations as low dissolved oxygen concentrations, leading to fermentative metabolism, are found in the upper part of the reactor. Time scales for oxygen transfer are in the range of 10 – 20 seconds based on the overall k_La-values whereas mixing times are in the range of 100 – 200 seconds in the simulations made in 100 – 1000 m^3 scale. Based on these simulations, improving the gas handling capacity and the liquid mixing especially in the axial direction would be preferred improvements in large scale reactors. The current model for liquid mixing is based on literature work validated up to reactors 30 m^3 so the simulation results up to 1000 m^3 are indicative. Furthermore, it cannot be applied for stirred draft tube reactors without determining new parameters specific for the impeller and draft tube configuration. Further research is planned on more rigorous assessment of the hydrodynamics of different reactor types – such as stirred tank and airlift reactors as well as large

scale OKTOP®9000 – and the application of microbial growth kinetics with the more accurate estimation of hydrodynamic and mass transfer conditions.

5 Conclusions

The effect of oxygen transfer conditions on the cell growth and metabolism of *Pichia pastoris* was studied by laboratory batch experiments and modelling the yeast growth. The model describes well the effect of oxygen availability on oxidative/fermentative metabolism of the yeast, and the correspondence with literature data and laboratory scale batch experiments is good on qualitative basis. The scale-up effects were studied by applying the growth model with one dimensional reactor scale model in which the effects of gas phase depletion, hydrostatic pressure and axial mixing of the dispersion were included. The model simulations indicated a decrease in cell yield when the size of the reactor was increased. The effect is mainly due to increased gas phase residence time and oxygen depletion in the gas phase, and insufficient mixing of the liquid phase. These effects lead to oxygen limited conditions for the yeast in some parts of the reactor and onset of fermentative metabolism. On the other hand, hydrostatic pressure increases with scale, which increases the partial pressure of oxygen and, thus, the driving force for mass transfer. Improvements in the gas handling capacity at moderate agitator power input, and improvement of overall liquid mixing of the reactor would significantly improve the reactor performance in large scale.

Acknowledgements

The authors acknowledge the Finnish Funding Agency for Innovation Tekes for providing financing for this work (Grant number 906/312016, Tackling mass transfer challenges in fermentations). The authors would also like to thank Stella Polido for her assistance in the experimental work.

References

Baumann, K., Carnicer, M., Dragosits, M., Graf, A.B., Stadlmann, J., Jouhten, P., Maaheimo, H., Gasser, B., Albiol, J., Mattanovich, D., Ferrer, P., 2010. A multi-level study of recombinant Pichia pastoris in different oxygen conditions. BMC Syst. Biol. 4, 141. https://doi.org/10.1186/1752-0509-4-141

475 Baumann, K., Maurer, M., Dragosits, M., Cos, O., Ferrer, P., Mattanovich, D., 2008. Hypoxic fed-
476 batch cultivation of Pichia pastoris increases specific and volumetric productivity of
477 recombinant proteins. Biotechnol. Bioeng. 100, 177–183. https://doi.org/10.1002/bit.21763
478 Carnicer, M., Baumann, K., Töplitz, I., Sánchez-Ferrando, F., Mattanovich, D., Ferrer, P., Albiol, J.,
479 2009. Macromolecular and elemental composition analysis and extracellular metabolite
480 balances of Pichia pastoris growing at different oxygen levels. Microb. Cell Factories 8, 65.
481 https://doi.org/10.1186/1475-2859-8-65
482 Carnicer, M., ten Pierick, A., van Dam, J., Heijnen, J.J., Albiol, J., van Gulik, W., Ferrer, P., 2012.
483 Quantitative metabolomics analysis of amino acid metabolism in recombinant Pichia
484 pastoris under different oxygen availability conditions. Microb. Cell Factories 11, 83.
485 https://doi.org/10.1186/1475-2859-11-83
486 Chisti, Y., Jauregui-Haza, U.J., 2002. Oxygen transfer and mixing in mechanically agitated airlift
487 bioreactors. Biochem. Eng. J. 10, 143–153.
488 Garcia-Ochoa, F., Gomez, E., 2009. Bioreactor scale-up and oxygen transfer rate in microbial
489 processes: An overview. Biotechnol. Adv. 27, 153–176.
490 Garcia-Ochoa, F., Gomez, E., Santos, V.E., Merchuk, J.C., 2010. Oxygen uptake rate in microbial
491 processes: An overview. Biochem. Eng. J. 49, 289–307.
492 Gezork, K.M., Bujalski, W., Cooke, M., Nienow, A.W., 2000. The transition from homogeneous to
493 heterogeneous flow in a gassed, stirred vessel. Chem. Eng. Res. Des. 78, 363–370.
494 https://doi.org/10.1205/026387600527482
495 Heijnen, J.J., 2005. Approximative kinetic formats used in metabolic network modeling. Biotechnol.
496 Bioeng. 91, 534–545. https://doi.org/10.1002/bit.20558
497 Ho, Y.K., Doshi, P., Yeoh, H.K., Ngoh, G.C., 2015. Interlinked population balance and cybernetic
498 models for the simultaneous saccharification and fermentation of natural polymers.
499 Biotechnol. Bioeng. 112, 2084–2105. https://doi.org/10.1002/bit.25616
500 Kerkhoven, E.J., Lahtvee, P.-J., Nielsen, J., 2015. Applications of computational modeling in
501 metabolic engineering of yeast. FEMS Yeast Res. 15, 1–13. https://doi.org/10.1111/1567-
502 1364.12199
503 Lueske, J., Kar, K., Piras, L., Pressler, J., 2015. Power Draw and Gas-Liquid Mass Transfer
504 Characteristics of a Stirred-Tank Reactor with Draft Tube Configuration. Chem. Eng. Technol.
505 Moo-Young, M., Chisti, Y., Vlach, D., 1993. Fermentation of cellulosic materials to mycoprotein
506 foods. Biotechnol. Adv. 11, 469–479.
507 Nauha, E.K., Visuri, O., Vermasvuori, R., Alopaeus, V., 2015. A new simple approach for the scale-up
508 of aerated stirred tanks. Chem. Eng. Res. Des. 95, 150–161.
509 https://doi.org/10.1016/j.cherd.2014.10.015
510 Oosterhuis, N.M.G., Kossen, N.W.F., 1984. Dissolved oxygen concentration profiles in a production-
511 scale bioreactor. Biotechnol. Bioeng. 26, 546–550. https://doi.org/10.1002/bit.260260522
512 Paul, E.L., Atiemo-Obeng, V.A., Kresta, S.M., 2004. Handbook of Industrial mixing : science and
513 practice. Wiley-Interscience, Hoboken, NJ :
514 Pollard, D.J., Ison, A.P., Shamlou, P.A., Lilly, M.D., 1997. Influence of a propeller on Saccharomyces
515 cerevisiae fermentations in a pilot scale airlift bioreactor. Bioprocess Eng. 16, 273–281.
516 Ramkrishna, D., Song, H.-S., 2012. Dynamic models of metabolism: Review of the cybernetic
517 approach. AIChE J. 58, 986–997. https://doi.org/10.1002/aic.13734

518 Solà, A., Maaheimo, H., Ylönen, K., Ferrer, P., Szyperski, T., 2004. Amino acid biosynthesis and
519 metabolic flux profiling of Pichia pastoris. Eur. J. Biochem. 271, 2462–2470.
520 https://doi.org/10.1111/j.1432-1033.2004.04176.x
521 Sonnleitner, B., Käppeli, O., 1986. Growth of Saccharomyces cerevisiae is controlled by its limited
522 respiratory capacity: Formulation and verification of a hypothesis. Biotechnol. Bioeng. 28,
523 927–937. https://doi.org/10.1002/bit.260280620
524 Tervasmäki, P., Latva-Kokko, M., Taskila, S., Tanskanen, J., 2016. Mass transfer, gas hold-up and cell
525 cultivation studies in a bottom agitated draft tube reactor and multiple impeller Rushton
526 turbine configuration. Chem. Eng. Sci. 155, 83–98.
527 https://doi.org/10.1016/j.ces.2016.07.048
528 Vrábel, P., van der Lans, R.G.J.M., Luyben, K.C.A.M., Boon, L., Nienow, A.W., 2000. Mixing in large-
529 scale vessels stirred with multiple radial or radial and axial up-pumping impellers: modelling
530 and measurements. Chem. Eng. Sci. 55, 5881–5896. https://doi.org/10.1016/S0009-
531 2509(00)00175-5
532